Department of Electrical Engineering,
Faculty of Engineering Science,
The University of Western Ontario,
London, Ontario. N6A 5B9

The Design and Operation of an Acoustic Radar and Analysis of Experimental Microwave Multipath Data.

A. R. Webster and W. Liu.

Final Report,
D.S.S. Contract #
36001-0-3535.

April 1991.

The Design and Operation of an Acoustic Radar

and

Analysis of Experimental Microwave Multipath Data.

A Final Report under
Department of Supply and Services
Contract # 36001-0-3535

submitted to

Communications Research Centre,
Department of Communications,
Ottawa, Ontario.

Principal Investigator: Dr. A. R. Webster, P.Eng.

Research Associate: Wei Liu.

April 1991

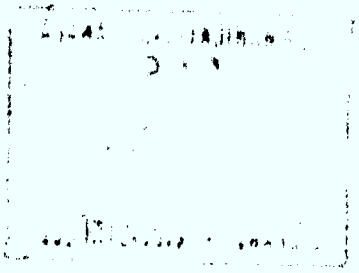

Contents.

1. Introduction

Over a period of several years, collaborative work in the field of microwave propagation between The University of Western Ontario (UWO) and the Communications Research Centre (CRC), with help from industrial partners such as Bell Canada, has established a substantial data base. As a result of a series of contracts, a wide-aperture microwave interferometer was developed and installed successively on several microwave links, the last being the Kemptville-Avonmore link of Bell Canada (DSS contract # 36001-9-3515). Continuation of these efforts with augmented observations was deemed to be desirable.

The objectives of the work described here were as follows:

1. To reactivate the microwave interferometer equipment already installed on the Bell Canada Kemptville-Avonmore microwave link.

2. To complete the design and construction of an acoustic radar system.

3. To operate this acoustic radar and the interferometer during the 1990 fading season in conjunction with CRC experiments.

4. To perform detailed statistical analyses of multiple ray observations made during 1988 and 1989.

The microwave system was successfully reactivated in August, 1990 and new data collected for a period of about two months. An accumulation of about 600 hours of data was obtained and stored on magnetic tape; of these data, approximately 60 hours of fading were observed. No further processing of these data has been done to date.

The acoustic radar was developed and deployed in 1990 at the Avonmore end of the link. Unfortunately, small problems with both hardware and software resulted in no meaningful data collection due to the lateness with respect to the fading season. The planned CRC experiments also hit snags so that no multi-experiment observations were possible in the 1990 fading season. The problems with the acoustic sounder have been fixed so that it is now ready for deployment.

Some further data analysis was carried out on the 1988/89 data from the microwave system on the Kemptville-Avonmore link.

2. The Acoustic Radar System

The principle behind this system is based on the fact that sound waves propagating in the atmosphere experience enhanced back-scattering when passing through a region where the (potential) temperature gradient in the direction of travel is higher than normal. This allows the probing of the lower atmosphere (up to a few hundred metres) using an acoustic radar technique in which short pulses of sound waves are transmitted vertically upwards resulting in "echoes" from layers which have large vertical temperature gradients. Such layers are also likely to produce anomalous microwave propagation, such as multipath; hence the interest in concurrent experimental measurements. Additional direct measurements of refractivity would provide invaluable data for any attempt to model the medium for microwave propagation and this area is the one in which CRC is directly involved.

The **sodar** (acronym referring to radar using sound) system has been designed to take advantage of the availability of inexpensive microcomputers which allows considerable flexibility of operation to be built-in. A low-end 8086 microcomputer is used and this has more than enough power to handle the task, which involves the following basic operations.

A short pulse of audio frequency power is radiated upwards. The speed of sound is about 330 m/s so that "echoes" are returned with time delay proportional to the height above ground; 1000 m. range corresponds to about 6 s. elapsed time. For a given fraction of power reflected, the returned echo amplitude is (approximately) inversely proportional to the range and the gain of the amplifier is increased in a linear fashion in time to compensate for this, i.e. for a given layer which would reflect a given fraction of the incident power, the amplitude of the echo at the receiver output is (ideally) constant over the chosen height range. Additional gain control is provided in order to allow optimization of the system under different ambient conditions and for different height ranges. The microcomputer has control of almost all of the variable parameters and these are reset before each sweep. One sweep consists of transmission of the audio pulse followed by a short interval (150 ms) of receiver blanking corresponding to 25 m. in height. Sampling of the receiver output then takes place at a fixed rate (set to 100/s. for now) for an interval corresponding to the desired height range (e.g. 3s. for a height range of 500 m.). In addition, the microcomputer determines the operating frequency, pulse width and system bandwidth. An overall block diagram of the system is shown in fig.1.

2.1 The Sodar Hardware.

The system hardware is divided into three separate sections with each section mounted on its own printed circuit board; a fourth board within the unit provides all of the necessary power. The division of the various functions amongst these boards is as shown in fig. 2.

The logic (or synthesizer) board provides all of the basic clock signals derived from a single crystal oscillator. The ramp clock is a fixed frequency (625 Hz) used to develop an analog voltage which controls the gain of the ramp amplifier on the receiver card. A Voltage Controlled Oscillator (VCO) is used to generate, under computer control, a signal at a frequency (f_r) 100 times the desired operating frequency (f_o). This signal (f_r) is used to operate narrow-band digital filters (MF8) on both the transmitting (TX) and receiving (RX) boards.

The transmitting board consists essentially of a dividing network and filter to generate the operating frequency signal followed by a gate arrangement which determines the "on" time of the transmitter. Further filtering and power amplification completes this section and the nominal 100W signal is fed directly to the (8W) transducer which serves as both loudspeaker and microphone for subsequent reception. It will be noted that the operating frequency (f_o) is only present for a short time straddling the "TX on" period so that no contamination of the received signal occurs during the time allotted for reception. The output stage of the power amplifier is permanently connected to the transducer, but presents a high impedance when not operating.

The receiver is also connected to the transducer but a relay is open when the transmitter is operating and remains open for a short period thereafter to protect the receiver from damage. The relay is closed after period of 150 ms from the start of the transmitter pulse (corresponding to a height of 25 m.) and a transformer is used to present a matched load to the receiver. A fixed high-gain amplifier follows this leading to the ramp amplifier and digital filter. A computer-controlled-gain amplifier (to allow final gain adjustment) and a detector completes the receiving board.

Communication between the computer and the above electronics is via an industry standard "Data Translation DT2808" analog/digital converter board, which handles the two-way digital traffic and the final analog signal from the receiver.

The layout of the mother board sockets for the three main electronics boards and the connection to the DT2808 is shown in fig. 3, and detailed schematics are to be found in fig. 4.

2.2 The Sodar Software.

The microcomputer controls the entire operation using software written in Turbo Pascal. On initial power up, the user establishes the desired parameter values using an interactive menu. The range of values is shown in Table 1.

Table 1.
System Parameters.

Operating Frequency	1.2	to	2.4	kHz
Pulse Length	20	to	70	ms.
Height Range		500 m. fixed*		
Pulse Repetition Period	12	to	60	sec.
Bandwidth	25	to	80	Hz.
Gain Factor	1	to	8	
Sampling Rate		100 /s. fixed*		

* these could be made variable at some later date if need be.

Once this is done, the user is led through a series of requests to establish the data recording timetable. This fixes the starting date and time of day, the finish date and time of day and whether or not continuous recording is to take place. The alternative is to stipulate the same period daily (e.g., 1700 on each day to 0900 on the next day) which allows longer unattended recording and/or minimization of possible disturbance to others (the nominal transmitted power of 100W is audible over a considerable distance).

The operation from this point on is automatic and the data is recorded in two ways. First, a "traditional" type of display is generated using a dot matrix printer and four "grey" levels represented by 0, 1, 2 or 3 dots. Such a record is shown in fig. 5 and serves to establish periods of time when layering in the lower atmosphere is occurring. The second means of recording the data involves sampling the analog

signal at a suitable rate (100 Hz nominal) for a period appropriate to the desired height range (3 sec. for 500 m.) and converting to 8-bit digital form. These "bytes" are then stored in files of suitable length on the computer hard disk drive. Currently, the file length is set to correspond to one hour of data, i.e. 100 samples/sec x 3 sec. x 200 sweeps/hour gives a file length of 60,000 bytes. This length of file is a compromise between storage efficiency and data loss should a power outage occur. Another limitation is the inability of Turbo Pascal to handle data arrays greater than 64 kbytes, although this can be circumvented. The file format (in bytes) is shown in fig. 6; the month day and year form the file name with the extension giving the hour. Once files totalling a chosen amount have been accumulated, they are transferred to cartridge magnetic tape in the drive installed in the computer. The nominal capacity of both hard drive and tape drive is 40 Mbytes. From this point, the raw data is available in digital form for further processing using digital techniques such as filtering, peak (i.e layer) detection etc.

The entire system has been tested successfully in the laboratory and now awaits field tests and evaluation.

3. Microwave Data Analysis and Results.

Further analysis of the microwave data collected in previous years on the Kemptville-Avonmore link has been performed with a view to looking at conditional statistics related to the angle-of-arrival of the strongest ray under multipath conditions. This is intended to augment the results reported previously (see Final Report D.S.S. Contract # 36001-8-3515).

As described in the above report, the data used in the analysis was selected from the overall data base by scanning visually a presentation of maximum, minimum and average values for each minute from each 9-track magnetic tape, the total capacity of each tape being about 88 hours of continuous recording. Complete hours in which significant fast fading was evident were included; fast fading exhibits relatively rapid changes in amplitude as opposed to general slow variations over an extended period. Visual scanning was used because of the difficulty of allowing for all contingencies (rain attenuation is one) in automatic computer scanning.

The rate of occurrence of such fast fading for the Kemptville-Avonmore link in 1988/89 is shown on fig. 7. Almost continuous recording was achieved for each month and the numbers presented have been normalised to a full month. The seasonal variation is apparent with July being (marginally) the worst fading month. The remaining analysis presented here concentrates on the 1989 data, with consideration being given to all of the 1989 data and to that of the worst fading month (July).

Previous analysis has looked at the disribution of various ray parameters conditional upon the amplitude of the strongest ray. Here, the emphasis is placed on distributions conditioned on the angle-of-arrival of the strongest ray **in a resolved multipath situation.** By this is meant that only records were used which, after initial processing using the Fast Fourier Transform, showed the existence of **at least 3 resolved rays** . A limit of 20 dB down from the amplitude of the strongest ray was imposed as before. The absolute limit on the resolution, due to finite antenna array aperture is about 0.1° while some degradation out to separations of 0.15° or so are to be expected. All of this, admittedly, is bound to colour the final results and the limitations should be borne in mind.

Fig. 8 shows distribution in AOA of the strongest ray (in 0.1° steps) for the two 1989 data sets and the corresponding median amplitude; the latter is derived from the distribution in amplitude for each 0.1° interval as shown in fig. 9. The overall range used here (-0.2° to +0.5°) for the strongest ray encompasses most of these rays with insignificant numbers outside of this range. The higher than normal median amplitude for elevated rays, at least in the interval 0.0° to 0.2°, is consistent with previous results and with the predictions of ray tracing. The low elevation strongest rays are few in number and depressed in amplitude. This may suggest broad defocussing effects or alternatively defocussing of the elevated rays to the point where ground reflected rays become dominant. More work is suggested here especially in the area of expected refractivity gradients close to the ground.

The angle-of-arrival distributions of the second and third strongest rays for the same 0.1° intervals in AOA of the strongest is shown in fig. 10 for the worst month data; the hatched rectangles represent the above 0.1° (strongest ray) interval and a reduced count is to be expected for at least an extra 0.1° either side of this due to the limited resolution of the system. The AOAs are all relative to the normal angle-of-arrival under single path conditions. It will be noted that the third strongest ray is consistently mainly from below the normal direction suggesting that ground reflections are the main origin, though significant numbers of high rays also occur in this category. The second strongest is often closest in AOA to the main ray and either above or below it depending on the AOA of this strongest one. This may be interpreted as interchange between the more direct ray and the strongest ray refracted by an atmospheric layer as the amplitudes of the two vary with perturbations in refractivity.

4. Discussion.

Because of time and other constraints, it proved to be impractical to carry out the planned multi-experiment observations in1990. However, equipment developments now appear to be at a stage where such activities are possible during the upcoming 1991 fading season. This would undoubtedly provide significant input in terms of realistic modelling of the refractive environment and would represent a major step forward in this work. As was noted earlier, the refractivity profile close to the ground will influence the importance of ground reflections in the context of defocussing and other refractive effects.

On the data analysis side, much remains to be done even with the data already collected and the plan is to continue with this work with a view to providing improved statistical data on the actual distributions of incoming rays and direct simulation of real microwave links.

Acknowledgments.

The continued involvement and help of Bell Canada in the use of their installations is gratefully acknowledged.

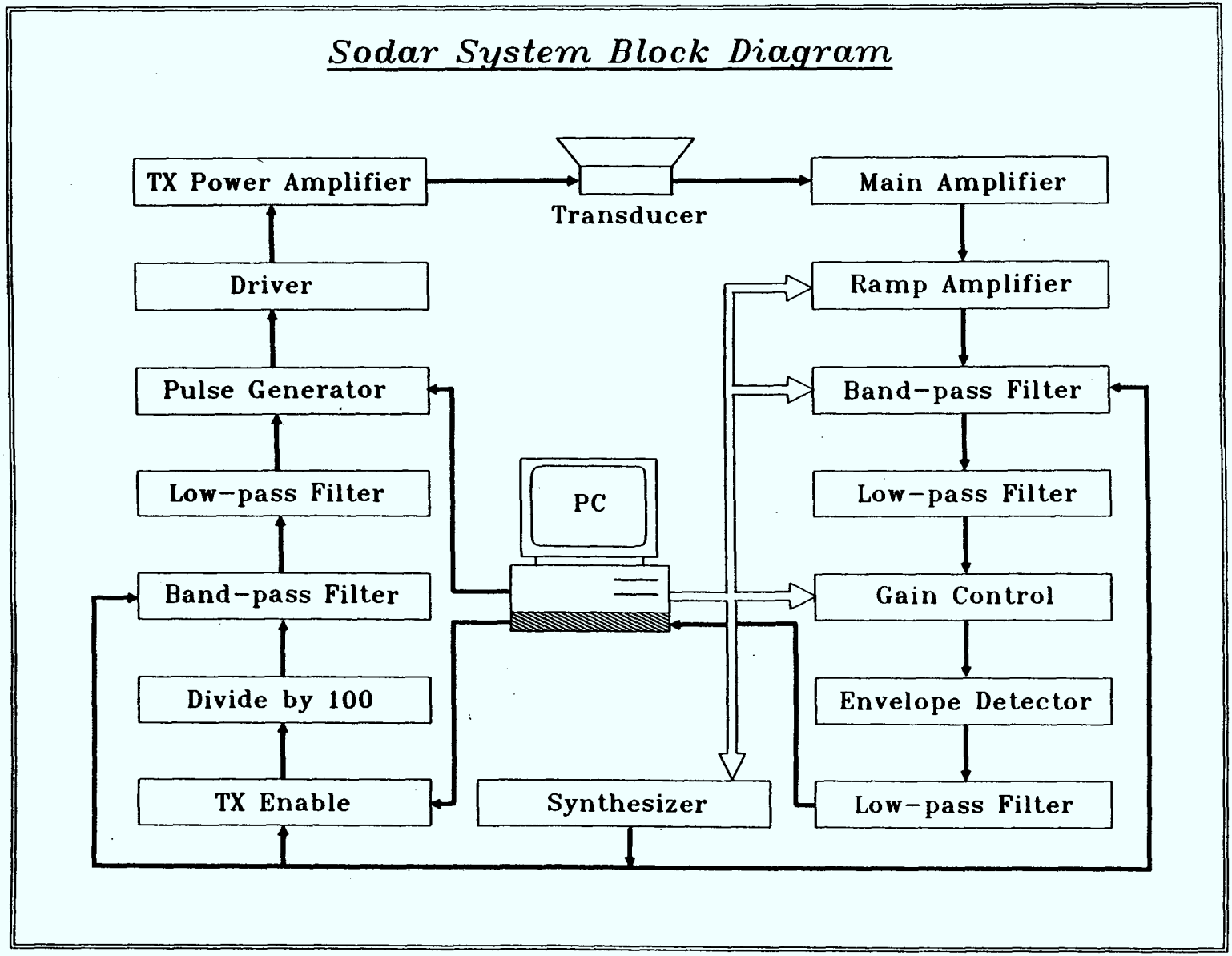

Fig. 1. The Sodar system block diagram.

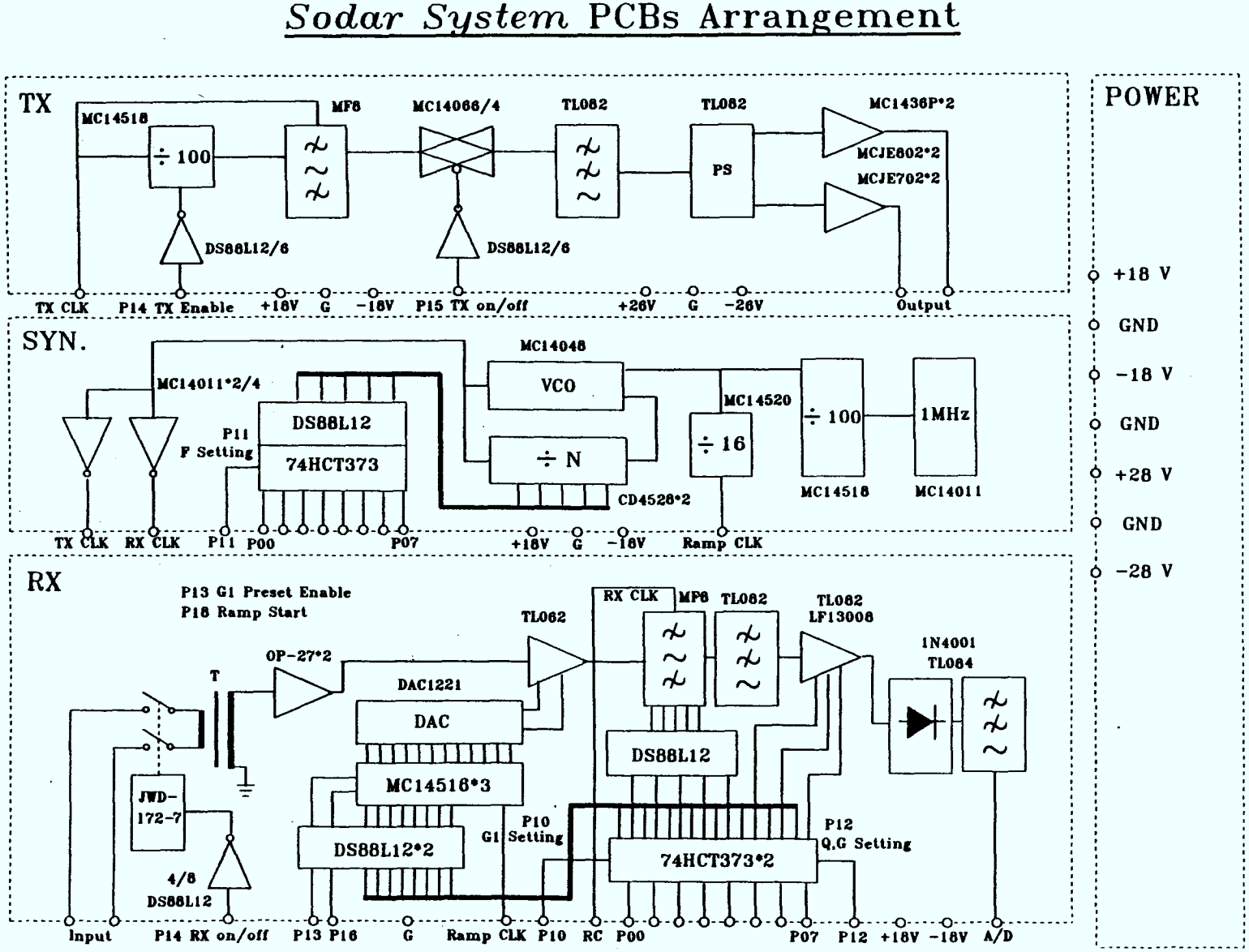

Fig. 2. Block diagrams of the three main printed circuit boards.

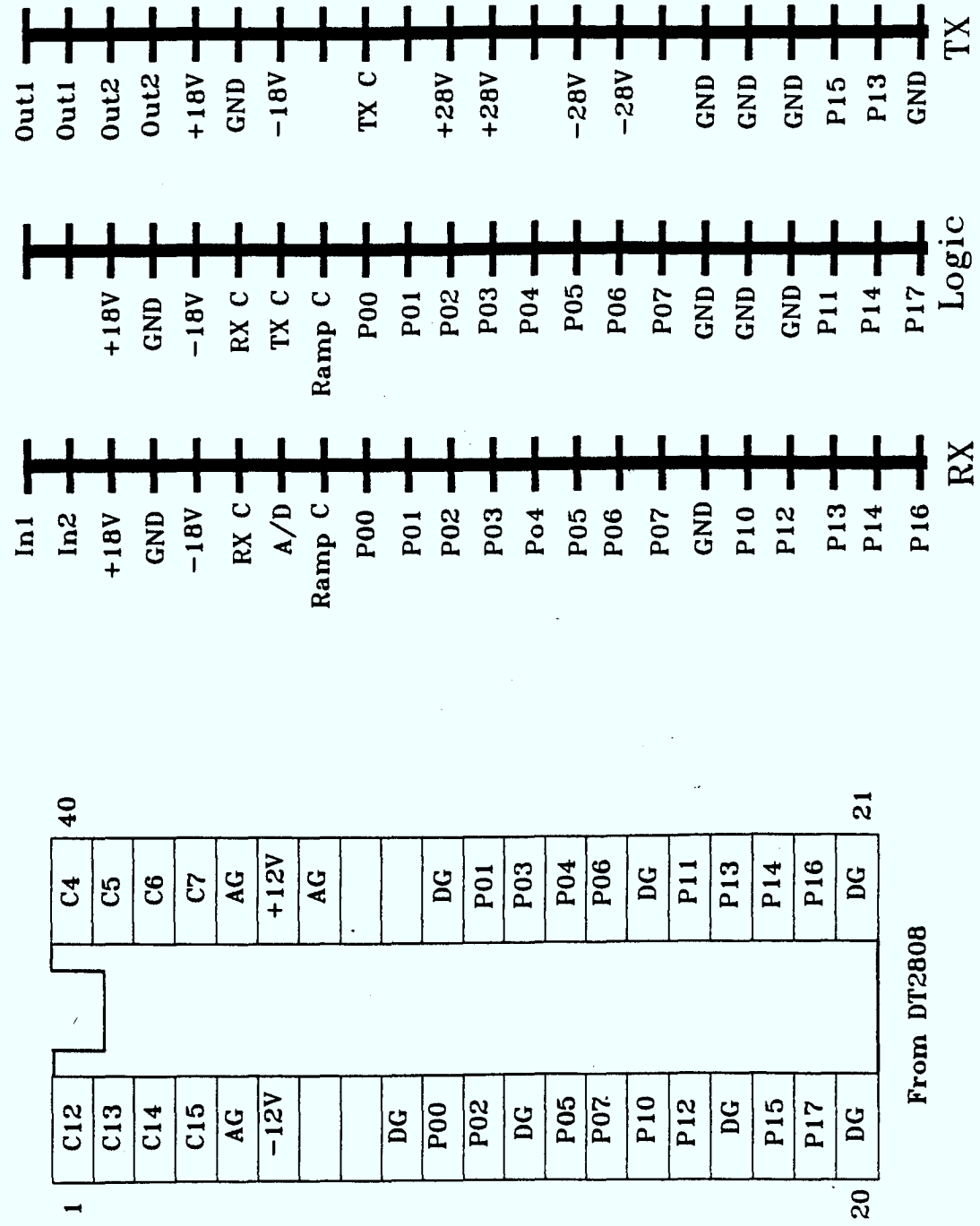

Fig. 3. The pin connections for the main boards and the A/D input/output socket.

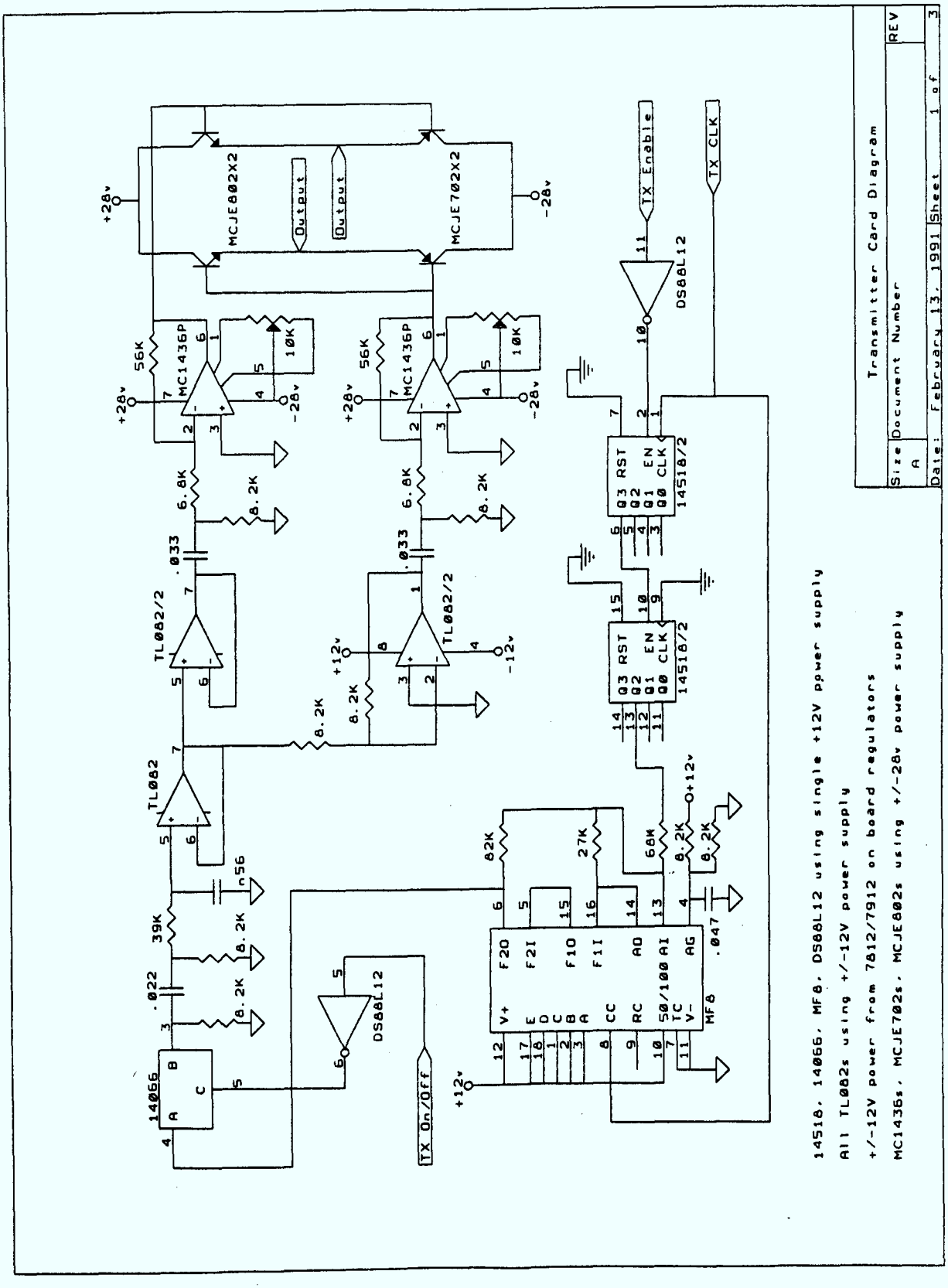

Fig. 4(a). Detailed schematic diagram of the transmitter board.

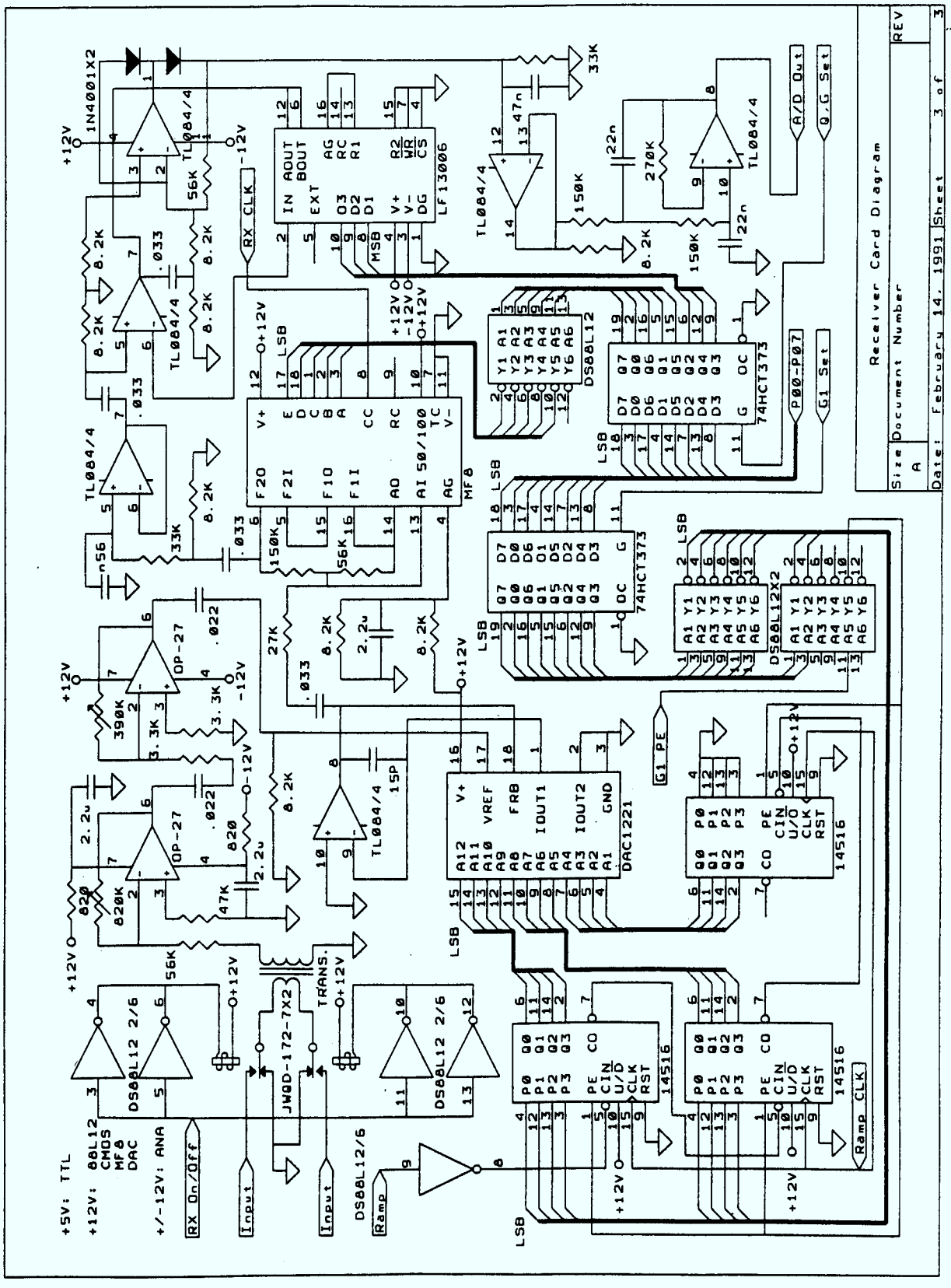

Fig. 4(b). Detailed schematic diagram of the Sodar receiver board.

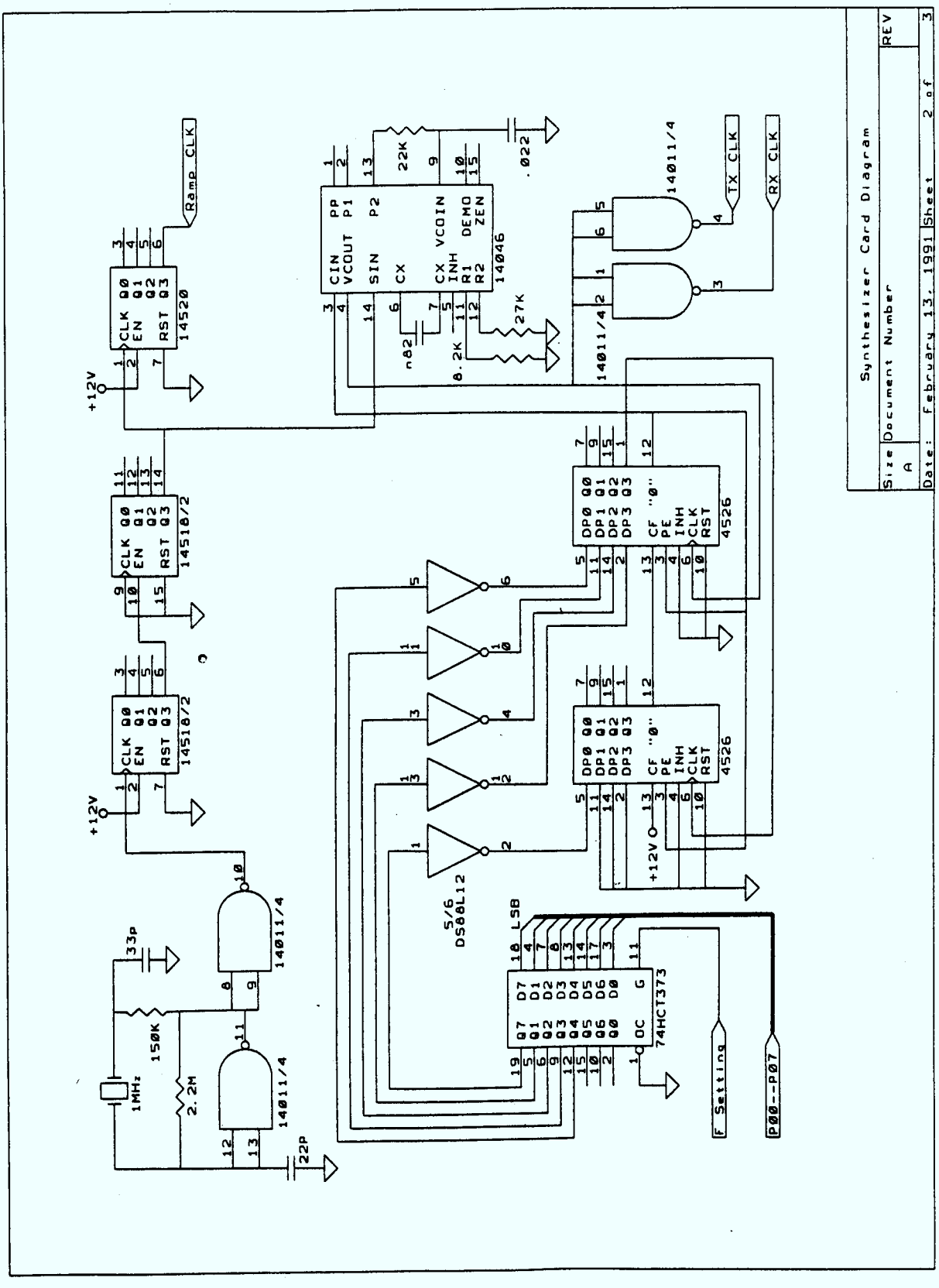

Fig. 4(c). Detailed Schematic Diagram of the Sodar Logic Board.

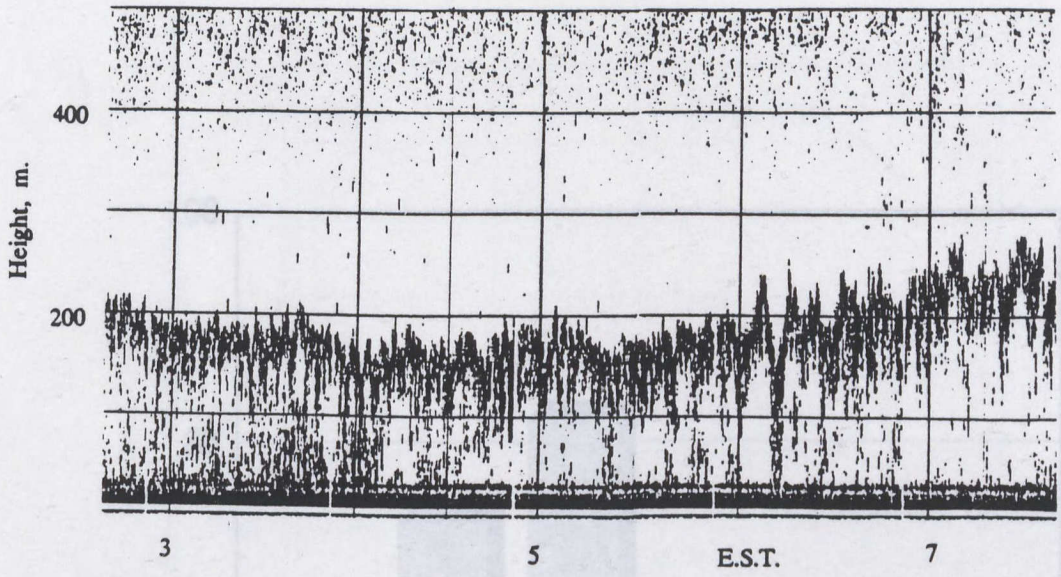

Fig. 5. The basic Sodar output display using a dot-matrix printer.

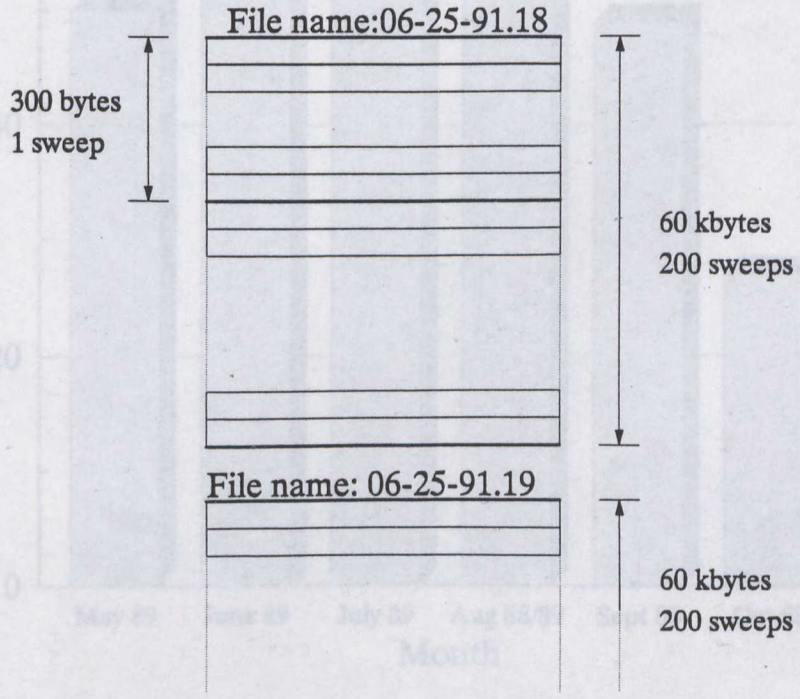

Fig. 6 The file storage scheme for the digitized data for each sweep.

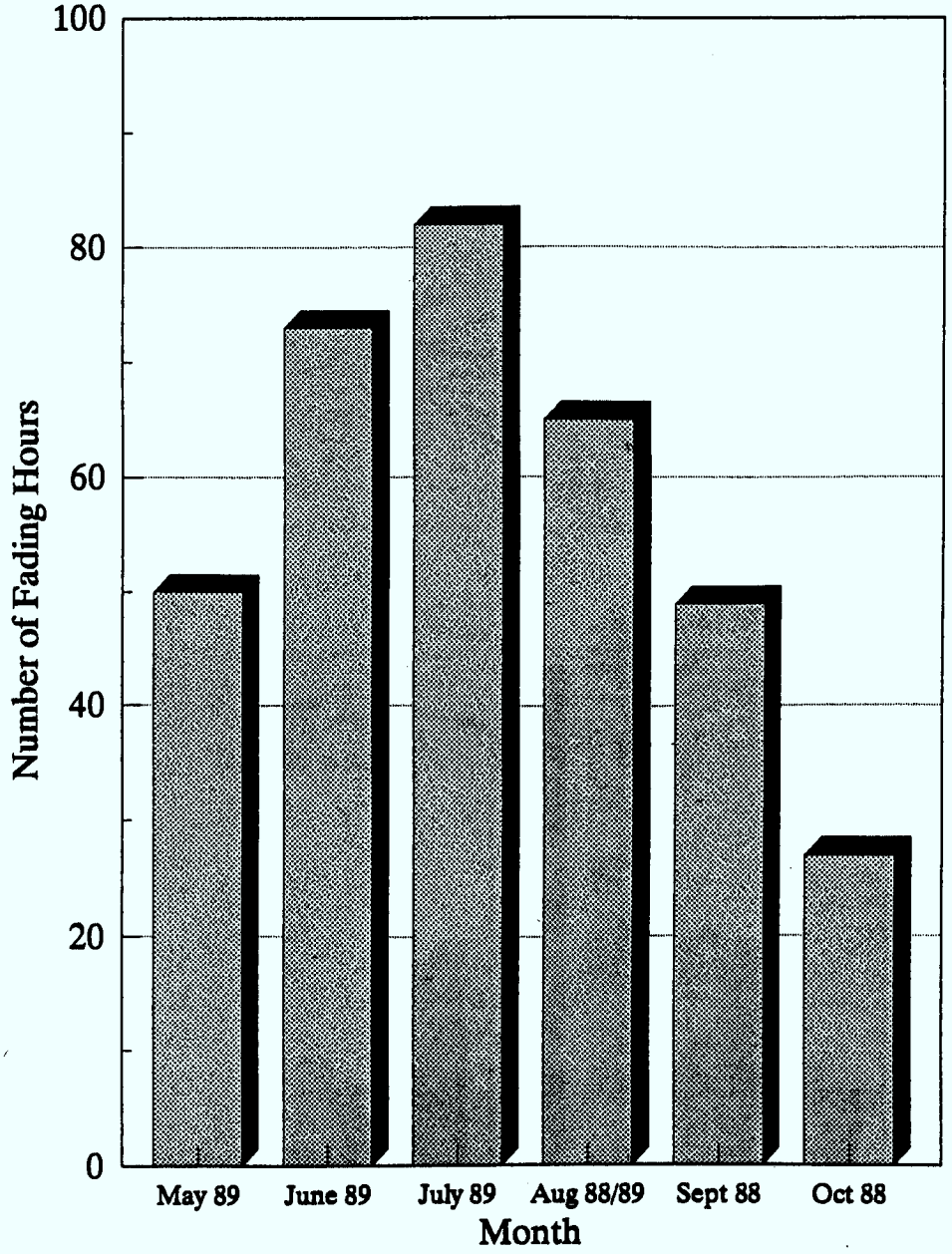

Fig. 7. The number of fading hours recorded in the indicated months. Recording was near to continuous and the data have been normalized to full months.

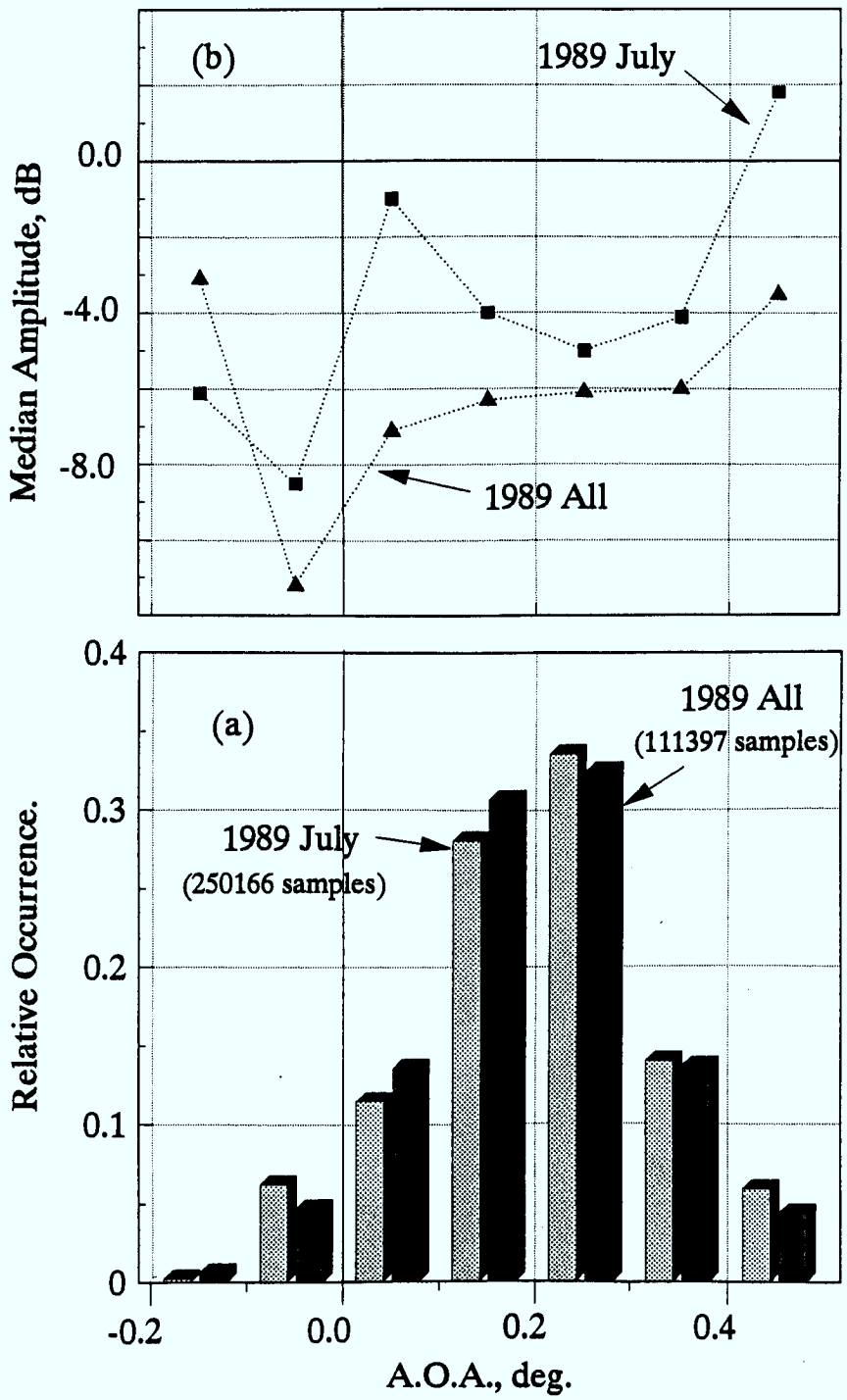

Fig. 8. (a) The relative occurrence of the strongest ray in each 0.1° interval for all of the 1989 data and the worst month and (b) the corresponding median amplitude.

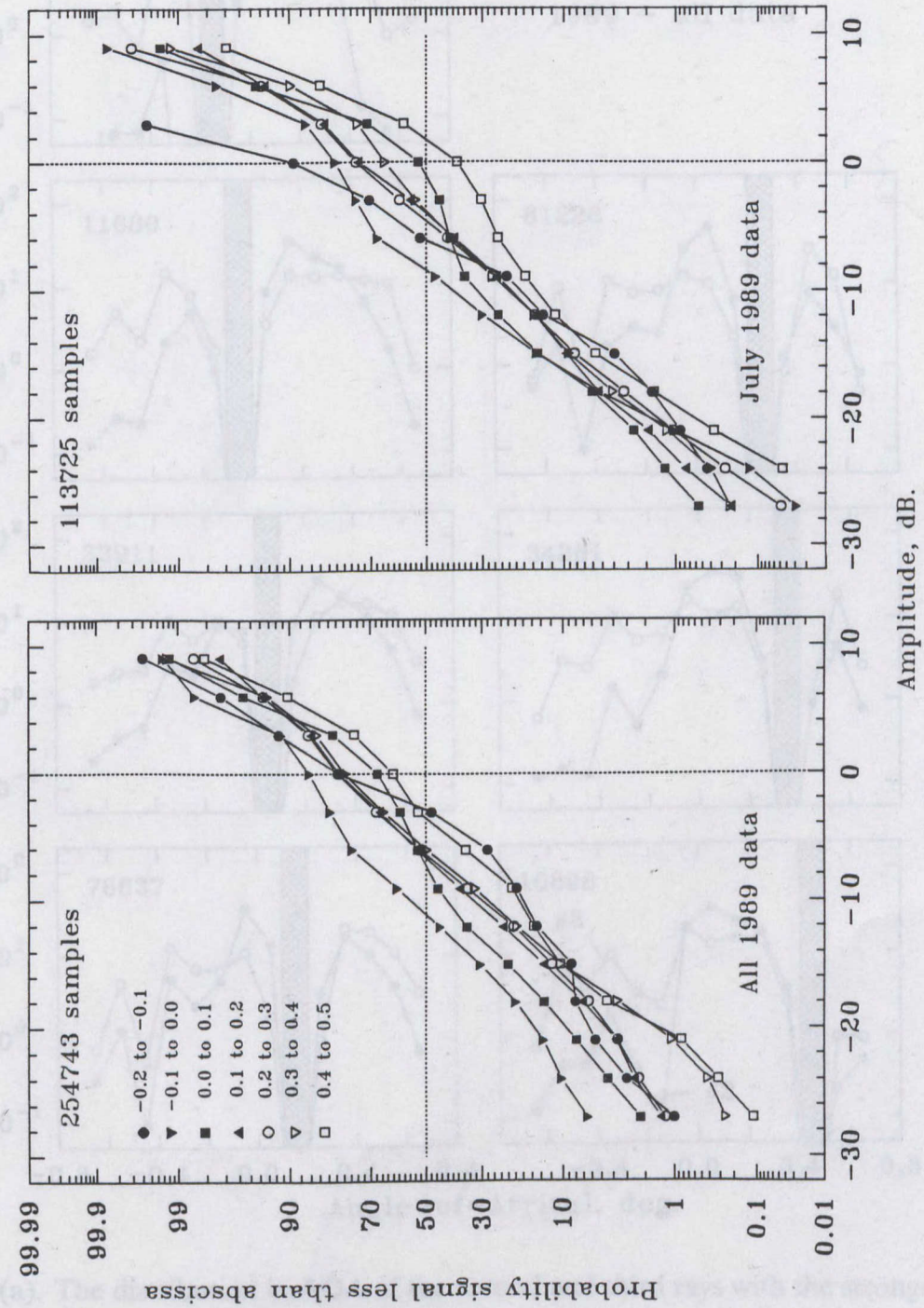

Fig. 9. Cumulative amplitude distributions for the strongest ray within each 0.1° interval for all 1989 data and for the worst month.

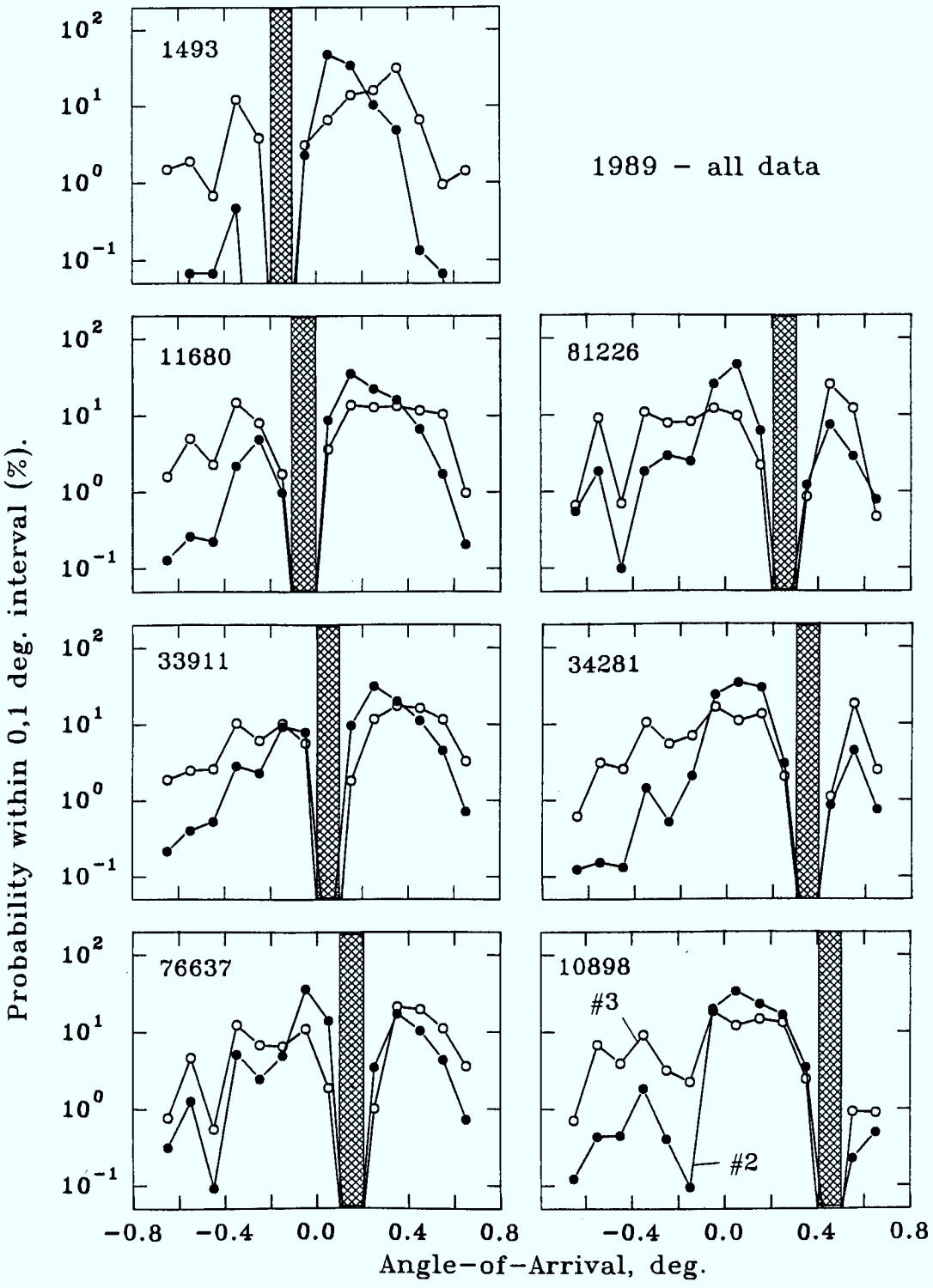

Fig.10(a). The distribution in AOA of the second and third rays with the strongest within the indicated (hatched rectangle) 0.1° AOA range; all 1989 data. The number of samples are as indicated.

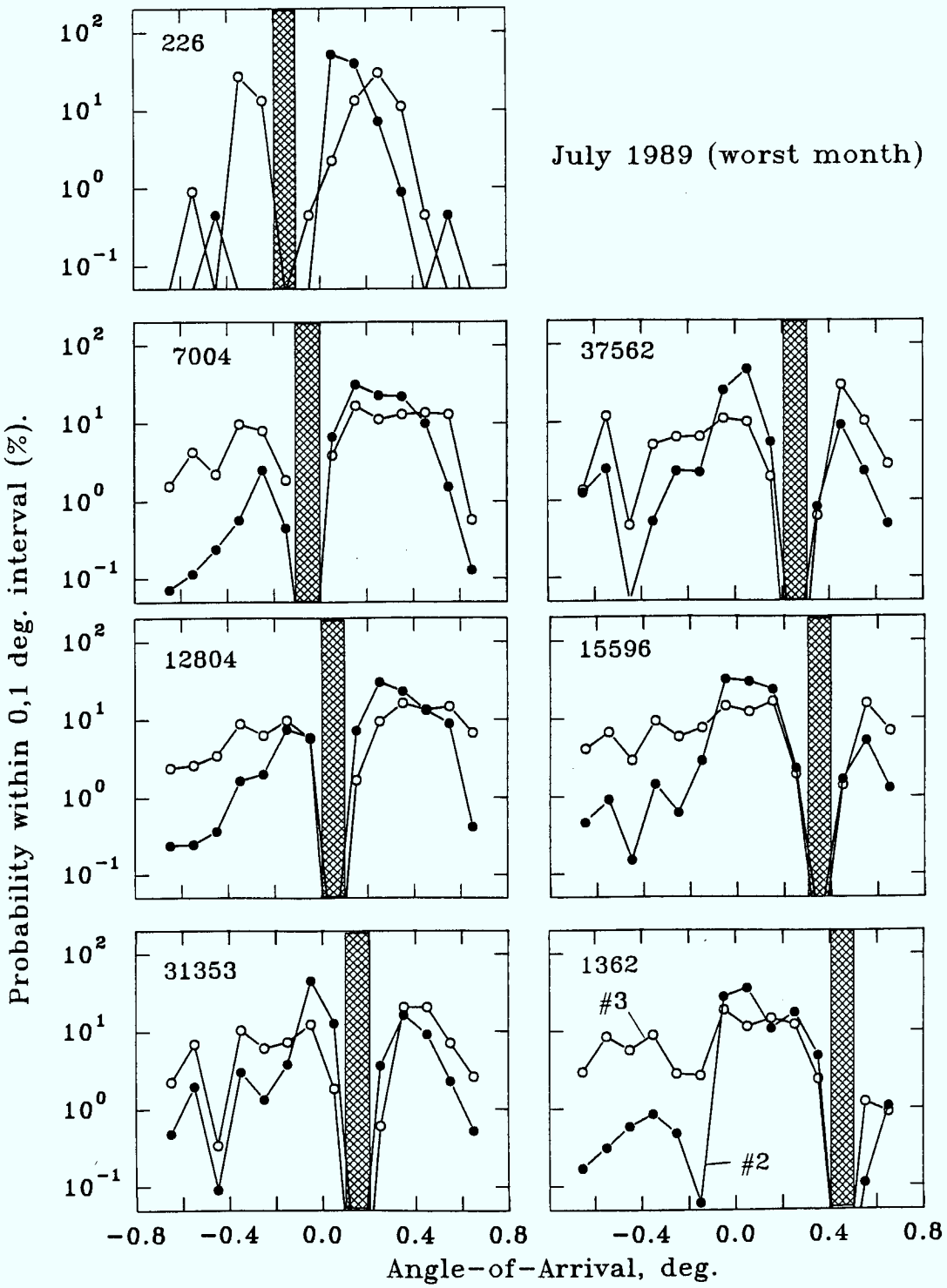

Fig.10(b). The distribution in AOA of the second and third rays with the strongest within the indicated (hatched rectangle) 0.1° AOA range; worst month.